Strong interaction of arbitrary fields of sound and light: Application to higher order Bragg imaging

K. Van Den Abeele, M. A. Breazeale, O. Leroy, and J. K. Na

Related Articles

Dual resonance excitation system for the contact mode of atomic force microscopy
Rev. Sci. Instrum. 83, 043703 (2012)

Fast scanning mode and its realization in a scanning acoustic microscope
Rev. Sci. Instrum. 83, 035113 (2012)

Angular measurement of acoustic reflection coefficients by the inversion of V(z, t) data with high frequency time-resolved acoustic microscopy
Rev. Sci. Instrum. 83, 014901 (2012)

Bragg grating writing in acoustically excited optical fiber
Appl. Phys. Lett. 97, 041101 (2010)

Method to improve the quality of acousto-optic imaging using an ultrashort and focused ultrasound pulse
Appl. Phys. Lett. 90, 121108 (2007)
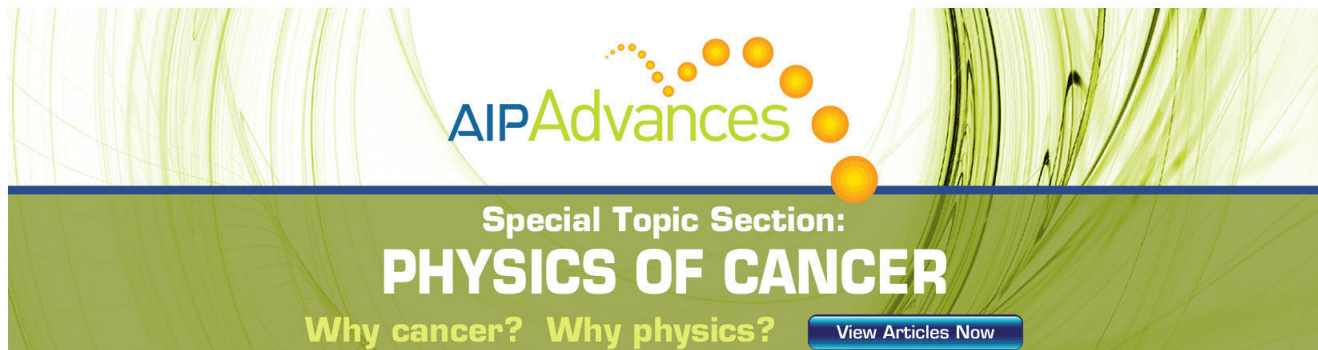
Additional information on J. Appl. Phys.

Journal Homepage: http://jap.aip.org/

Journal Information: http://jap.aip.org/about/about_the_journal

Top downloads: http://jap.aip.org/features/most_downloaded

Information for Authors: http://jap.aip.org/authors

Strong interaction of arbitrary fields of sound and light: Application to higher-order Bragg imaging

K. Van Den Abeele[a]
K. U. Leuven Campus Kortrijk, Interdisciplinary Research Center, B-8500 Kortrijk, Belgium

M. A. Breazeale
National Center for Physical Acoustics, University of Mississippi, University, Mississippi 38677,
and Department of Physics, The University of Tennessee, Knoxville, Tennessee 37996-1200

O. Leroy
K. U. Leuven Campus Kortrijk, Interdisciplinary Research Center, B-8500 Kortrijk, Belgium

J. K. Na
National Center for Physical Acoustics, University of Mississippi, University, Mississippi 38677,
and Department of Physics, The University of Tennessee, Knoxville, Tennessee 37996-1200

Small objects positioned in a high-frequency ultrasonic beam can be imaged by Bragg diffraction of light. The first order contains one image. Using a light beam with a considerable convergence angle and reducing the ultrasonic frequency, one observes that the second diffraction order contains two adjoining images, the third order three, etc., and that the positive orders are the mirror images of the negative ones. These experimental observations are explained by the present theory and general expressions for the angular distribution of the light in the different diffraction orders are presented in the form of a series expansion. Evidence for the multiple images in the higher diffraction orders is found by analyzing the first term in this expansion. The center-to-center separation of the images within the higher orders is found to be proportional to the ultrasonic frequency and the interaction width.

I. INTRODUCTION

In the study of the diffraction of light by ultrasound, quite a number of mathematical models can be used to predict accurately the diffraction direction, frequency shift, and intensity of the various orders which build up the pattern.[1-4] Applications of these models can be found in telecommunication, optical signal processing, optical computing, and nondestructive testing. Most models concentrate on describing and analyzing the diffraction effects for a known shape and time history of the ultrasonic wave. Only a few contributions have been published in which a reconstruction method for the diffracting sound wave is proposed and established. Some of these models include time or space reconstruction in the Raman–Nath regime of acousto-optic interaction;[5-12] others use the more common Bragg diffraction to visualize the cross section of a sound beam.[13,14] Whereas the Raman–Nath regime requires extensive data analysis for cross-sectional mapping, Bragg imaging has the advantage of copying all information exactly at once in the first diffraction order.

A means of studying Bragg imaging was developed first by Korpel. He showed that objects placed in the ultrasonic beam were imaged in the first diffraction order and explained the results in terms of ray optics.[13] Later Korpel explained the mapping by considering the Bragg diffraction process as one of parametric mixing.[14] Using Fourier analysis and the formalism of Feynman diagrams, Korpel and Poon[15-17] developed a theory for strong acousto-optic in-

teraction where both the light and sound fields are accurately represented by their plane-wave decomposition together with multiple scattering. They investigated the usefulness and validity of this approach by deriving limit case expressions for plane-wave Raman–Nath and Bragg diffraction. The analysis of the solutions for arbitrary light and sound field distribution, however, heretofore has been limited to extreme Bragg conditions involving only two diffraction orders (order zero and plus or minus one).[18,19]

In 1971, Martin, Adler, and Breazeale[20] reported the experimental observation of multiple images in higher-order Bragg diffraction. Using a light beam with a considerable convergence angle and reducing the ultrasonic frequency, they were able to generate a one-to-one mapping in the first order together with a double mapping in the second diffraction order, and a triple mapping of the sound beam in the third order (see Fig. 1). By using a transmission plate as a frequency filter, Martin and co-workers proved that multiple images in the higher diffraction orders are not the result of nonlinear properties of the medium. Their theoretical explanation for multiple Bragg scattering was based on the imaging results for the first diffraction order, but is not in depth enough to describe all of the observed diffraction effects, e.g., the linear frequency and width dependence of the separation between two images in the higher orders. Na[21] gave another explanation based on the plane-wave theory of Blomme and Leroy,[2] but his model never includes the notion of profiled sound and therefore is incomplete as well.

In this work, we present a theoretical study of multiple Bragg imaging by investigating the interaction of a multi-
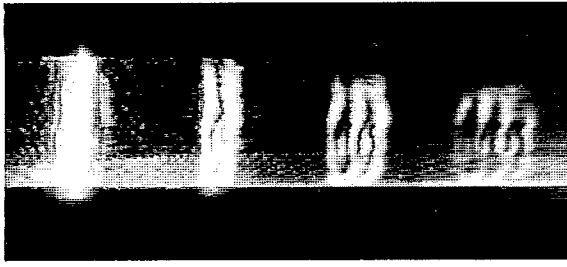
FIG. 1. Photograph showing single, double, and triple mapping of a loop in the first, second, and third diffraction orders of a convergent light beam by an ultrasonic wave at 10 MHz frequency (Ref. 20).

FIG. 2. General geometry for the interaction of profiled light and sound.

directional light beam and a profiled sound beam. Starting from the spectral decomposition of sound and light beams, we obtain a series expansion for the angular spectrum of any diffraction order by means of a backsubstitution method, introduced by Aggarwal[22] in 1950 for plane light wave diffraction by plane continuous ultrasonic waves. This allows us to find evidence for the appearance of mirror images. Analyzing the first term in the series expansion valid for high ultrasonic frequencies, we explain the generation of multiple adjoining images in the higher orders and examine the center-to-center separation of the images within these higher diffraction orders as a function of ultrasonic frequency and transducer width.

II. THEORY

A. Raman–Nath system for arbitrary light-sound interaction

Taking the Maxwell equations as a starting point, it can be shown that the diffraction process of a light beam by an ultrasonic grating is totally determined by the solution of following set of equations:[23]

$$E(x,z,t) = \Psi(x,z,t)e^{i\omega t}, \tag{1a}$$

$$\frac{\partial^2 \Psi}{\partial x^2}(x,z,t) + \frac{\partial^2 \Psi}{\partial z^2}(x,z,t) = -k^2 n^2(x,z,t)\Psi(x,z,t). \tag{1b}$$

In these diffraction equations, E is the magnitude of the electric field of the light with linear polarization in the y direction, ω is the circular frequency ($=2\pi\nu$), k is the propagation constant of the light beam in vacuum ($=2\pi/\lambda$ in which λ is the wavelength, also referring to vacuum), and n the time- and space-dependent refractive index induced by the presence of the ultrasonic wave. Throughout the text, the electrical engineering phasor convention is used with time dependence $\exp(i\omega t)$, where $i^2 = -1$. A general scheme of the interaction of profiled light and sound together with the coordinate system used in this study is illustrated in Fig. 2, where we identify the propagation direction of the sound beam with the x axis. We assume that the propagating sound beam profile does not change within the interaction region where it is illuminated by the light beam.

We want to investigate a sound profile at $x = x_0$ for which the amplitude is nonzero only within the range
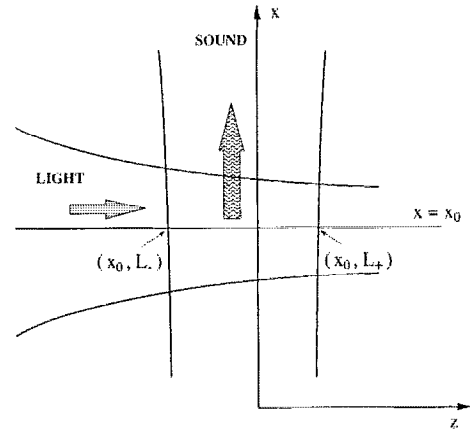
(L_-, L_+) along the z axis. The electric fields of the incident light and the sound beam distribution as a function of $\xi = x - x_0$ may then be represented by their angular plane-wave spectra,

$$E_{\text{inc}}(\xi, z, t) = \Psi_{\text{inc}}(\xi, z)e^{i\omega t}, \tag{2a}$$

with

$$\Psi_{\text{inc}}(\xi, z) = \int_{-\infty}^{+\infty} \widetilde{\Psi}_{\text{inc}}(n_0 k_x)e^{-in_0 k_z z}e^{-in_0 k_x \xi}\, dn_0\, k_x, \tag{2b}$$

where

$$\widetilde{\Psi}_{\text{inc}}(n_0 k_x) = \frac{e^{in_0 k_x L_-}}{2\pi} \int_{-\infty}^{+\infty} \Psi_{\text{inc}}(\xi, L_-)e^{in_0 k_x \xi}\, d\xi \tag{2c}$$

and

$$S(\xi, z) = \int_{-\infty}^{+\infty} \widetilde{S}(K_z)e^{-iK_z z}e^{-iK_x \xi}\, dK_z, \tag{3a}$$

with

$$\widetilde{S}(K_z) = \frac{i}{2\pi} \int_{-\infty}^{+\infty} S(0, z)e^{iK_z z}\, dz, \tag{3b}$$

so that the refractive index of the medium in which the sound wave propagates can be expressed as

$$n(\xi, z, t) = n_0 - \frac{i}{2}\hat{n}[S(\xi, z)e^{i\Omega t} - S^*(\xi, z)e^{-i\Omega t}], \tag{3c}$$

with n_0 the refractive index of the undisturbed medium, $\hat{n}$ the maximum variation in time and space, and Ω the ultrasonic circular frequency ($=2\pi F$). The universal notations $k_z^2 = k^2 - k_x^2$ and $K_x^2 = K^2 - K_z^2$ are used, with K the propagation constant of the ultrasound. The superscript $*$ stands for the complex conjugate operation.

The refractive index being periodic in time, we can express the solution of the diffraction equation (1b) as a Fourier series with the same periodicity,

$$\Psi(\xi, z, t) = \sum_{m=-\infty}^{+\infty} e^{im\Omega t}\Psi_m(\xi, z), \tag{4a}$$

in which we can represent each diffraction order by its spectral decomposition,

$$\Psi_m(\xi,z) = \int_{-\infty}^{+\infty} \widetilde{\Psi}_m(n_0 k_x, z) e^{-in_0 k_z z} e^{-in_0 k_x \xi}\, dn_0\, k_x. \quad (4b)$$

Introducing Eqs. (3) and (4) into Eq. (1b), straightforward calculation (neglecting second-order terms in $\hat{n}$, and taking into account the boundary conditions at $z = L_-$) leads to the following system of coupled integral equations for the interaction of both arbitrary light and sound fields:

$$\widetilde{\Psi}_m(n_0 k_x, z) - \widetilde{\Psi}_{\rm inc}(n_0 k_x)\delta_{m,0} = \frac{k^2 n_0 \hat{n}}{2} \int_{L_-}^{z} \int_{-\infty}^{+\infty} \frac{\widetilde{S}^*(K_z)\widetilde{\Psi}_{m+1}(n_0 k_x + K_x, z')}{Z(n_0 k_x)} e^{iz'[K_z - Z(n_0 k_x + K_x) + Z(n_0 k_x)]}\, dK_z\, dz'$$

$$-\frac{k^2 n_0 \hat{n}}{2} \int_{L_-}^{z} \int_{-\infty}^{+\infty} \frac{\widetilde{S}(K_z)\widetilde{\Psi}_{m-1}(n_0 k_x - K_x, z')}{Z(n_0 k_x)} e^{-iz'[K_z + Z(n_0 k_x - K_x) - Z(n_0 k_x)]}\, dK_z\, dz'. \quad (5)$$

In Eq. (5) we introduced the notation $Z(s) = \sqrt{n_0 k^2 - s^2}$, where the variable s of the functional Z can be equal to $n_0 k_x$ or $n_0 k_x \pm K_x$, and we continue to use this notation with sometimes even more complicated values for s throughout the text. As carefully indicated in Ref. 24, we empasize that $\widetilde{\Psi}$ denotes the virtual plane-wave spectrum with phase reference at the origin and not the local plane-wave spectrum.

B. General expressions for the light distribution in the diffraction orders

The solution of this Raman–Nath system of coupled equations at $z = L_+$ gives the Fourier-transformed amplitudes of the light distribution in the various diffraction orders behind the interaction zone. General expressions for $\widetilde{\Psi}_m(n_0 k_x, L_+)$ can be found by applying the backsubstitution method for consecutive approximations.[22]

In the first step we suppose that no light is diffracted, which means that

$$\widetilde{\Psi}_m \equiv 0 \quad \text{for } |m| \geqslant 1.$$

The solution for $m = 0$ then becomes

$$\widetilde{\Psi}_0(n_0 k_x, L_+) = \widetilde{\Psi}_{\rm inc}(n_0 k_x), \quad (6)$$

meaning that indeed all incident light is located in the undiffracted order.

Step 2 assumes that $\widetilde{\Psi}_0(n_0 k_x, L_+)$ is known from the first step and that one needs to consider only the undiffracted light and the plus and minus first diffraction orders. The solutions for $\widetilde{\Psi}_1$ and $\widetilde{\Psi}_{-1}$ then can be expressed in the form of double integrals,

$$\widetilde{\Psi}_1(n_0 k_x, L_+)$$

$$= -\frac{k^2 n_0 \hat{n}}{2} \int_{L_-}^{L_+} \int_{-\infty}^{+\infty} \frac{\widetilde{S}(K_z)\widetilde{\Psi}_{\rm inc}(n_0 k_x - K_x)}{Z(n_0 k_x)}$$

$$\times e^{-iz'[K_z + Z(n_0 k_x - K_x) - Z(n_0 k_x)]}\, dK_z\, dz', \quad (7a)$$

$$\widetilde{\Psi}_{-1}(n_0 k_x, L_+)$$

$$= \frac{k^2 n_0 \hat{n}}{2} \int_{L_-}^{L_+} \int_{-\infty}^{+\infty} \frac{\widetilde{S}^*(K_z)\widetilde{\Psi}_{\rm inc}(n_0 k_x + K_x)}{Z(n_0 k_x)}$$

$$\times e^{iz'[K_z - Z(n_0 k_x + K_x) + Z(n_0 k_x)]}\, dK_z\, dz', \quad (7b)$$

which can also be rewritten

$$\widetilde{\Psi}_1(n_0 k_x, L_+)$$

$$= -\frac{k^2 n_0 \hat{n}}{2} \int_{-\infty}^{+\infty} \frac{\widetilde{S}(K_z)\widetilde{\Psi}_{\rm inc}(n_0 k_x - K_x)}{Z(n_0 k_x)}$$

$$\times I_1^-(K_z, n_0 k_x, L_+)\, dK_z, \quad (7c)$$

where

$$I_1^-(K_z, n_0 k_x, L_+) = \int_{L_-}^{L_+} e^{-iz' A(K_z, n_0 k_x)}\, dz'$$

and

$$A(K_z, n_0 k_x) = K_z + Z(n_0 k_x - K_x) - Z(n_0 k_x),$$

$$\widetilde{\Psi}_{-1}(n_0 k_x, L_+)$$

$$= \frac{k^2 n_0 \hat{n}}{2} \int_{-\infty}^{+\infty} \frac{\widetilde{S}^*(K_z)\widetilde{\Psi}_{\rm inc}(n_0 k_x + K_x)}{Z(n_0 k_x)}$$

$$\times I_1^+(K_z, n_0 k_x, L_+)\, dK_z, \quad (7d)$$

where

$$I_1^+(K_z, n_0 k_x, L_+) = \int_{L_-}^{L_+} e^{iz' B(K_z, n_0 k_x)}\, dz'$$

and

$$B(K_z, n_0 k_x) = K_z - Z(n_0 k_x + K_x) + Z(n_0 k_x).$$

In the next step we assume that all diffraction fields with $|m| \geqslant 3$ are too weak to be detected, and that the expressions for the spectral decomposition of the plus and minus first orders follows the results deduced in step 2. This allows us to find the solutions for the second diffraction orders as quadruple integral expressions and to calculate a correction for the zeroth-order expression given in step 1:

$$\widetilde{\Psi}_2(n_0k_x,L_+) = \left(\frac{k^2n_0\hat{n}}{2}\right)^2 \int_{-\infty}^{+\infty}\int_{-\infty}^{+\infty} \frac{\widetilde{S}(K_z)\widetilde{S}(K_z')\widetilde{\Psi}_{\text{inc}}(n_0k_x-K_x-K_x')}{Z(n_0k_x)Z(n_0k_x-K_x)} I_2^{--}(K_z,K_z',n_0k_x,L_+)dK_z'\,dK_z, \tag{8a}$$

$$\widetilde{\Psi}_{-2}(n_0k_x,L_+) = \left(\frac{k^2n_0\hat{n}}{2}\right)^2 \int_{-\infty}^{+\infty}\int_{-\infty}^{+\infty} \frac{\widetilde{S}^*(K_z)\widetilde{S}^*(K_z')\widetilde{\Psi}_{\text{inc}}(n_0k_x+K_x+K_x')}{Z(n_0k_x)Z(n_0k_x+K_x)} I_2^{++}(K_z,K_z',n_0k_x,L_+)dK_z'\,dK_z, \tag{8b}$$

$$\widetilde{\Psi}_0(n_0k_x,L_+) = \widetilde{\Psi}_{\text{inc}}(n_0k_x) - \left(\frac{k^2n_0\hat{n}}{2}\right)^2 \int_{-\infty}^{+\infty}\int_{-\infty}^{+\infty} \frac{\widetilde{S}^*(K_z)\widetilde{S}(K_z')\widetilde{\Psi}_{\text{inc}}(n_0k_x+K_x-K_x')}{Z(n_0k_x)Z(n_0k_x+K_x)} I_2^{+-}(K_z,K_z',n_0k_x,L_+)dK_z'\,dK_z$$

$$-\left(\frac{k^2n_0\hat{n}}{2}\right)^2 \int_{-\infty}^{+\infty}\int_{-\infty}^{+\infty} \frac{\widetilde{S}(K_z)\widetilde{S}^*(K_z')\widetilde{\Psi}_{\text{inc}}(n_0k_x-K_x+K_x')}{Z(n_0k_x)Z(n_0k_x-K_x)} I_2^{-+}(K_z,K_z',n_0k_x,L_+)dK_z'\,dK_z, \tag{9}$$

with

$$I_2^{--}(K_z,K_z',n_0k_x,L_+) = \int_{L_-}^{L_+} e^{-iz'A(K_z,n_0k_x)}\int_{L_-}^{z'} e^{-iz''A(K_z',n_0k_x-K_x)}\,dz''\,dz',$$

$$I_2^{++}(K_z,K_z',n_0k_x,L_+) = \int_{L_-}^{L_+} e^{iz'B(K_z,n_0k_x)}\int_{L_-}^{z'} e^{iz''B(K_z',n_0k_x+K_x)}\,dz''\,dz',$$

$$I_2^{+-}(K_z,K_z',n_0k_x,L_+) = \int_{L_-}^{L_+} e^{iz'B(K_z,n_0k_x)}\int_{L_-}^{z'} e^{-iz''A(K_z',n_0k_x+K_x)}\,dz''\,dz',$$

and

$$I_2^{-+}(K_z,K_z',n_0k_x,L_+) = \int_{L_-}^{L_+} e^{-iz'A(K_z,n_0k_x)}\int_{L_-}^{z'} e^{iz''B(K_z',n_0k_x-K_x)}\,dz''\,dz'.$$

In step 4 we can calculate an expression for the third diffraction orders (both plus and minus) and correct the expressions for the first-order spectral decompositions by assuming the representation of $\widetilde{\Psi}_0$, $\widetilde{\Psi}_2$, and $\widetilde{\Psi}_{-2}$ as given in step 3. Restricting ourselves to the positive diffraction orders, we obtain the following formulas for $\widetilde{\Psi}_3$ and $\widetilde{\Psi}_1$:

$$\widetilde{\Psi}_3(n_0k_x,L_+) = -\left(\frac{k^2n_0\hat{n}}{2}\right)^3 \int_{-\infty}^{+\infty}\int_{-\infty}^{+\infty}\int_{-\infty}^{+\infty} \frac{\widetilde{S}(K_z)\widetilde{S}(K_z')\widetilde{S}(K_z'')\widetilde{\Psi}_{\text{inc}}(n_0k_x-K_x-K_x'-K_x'')}{Z(n_0k_x)Z(n_0k_x-K_x)Z(n_0k_x-K_x-K_x')}$$

$$\times I_3^{---}(K_z,K_z',K_z'',n_0k_x,L_+)dK_z''\,dK_z'\,dK_z, \tag{10}$$

$$\widetilde{\Psi}_1(n_0k_x,L_+) = -\frac{k^2n_0\hat{n}}{2}\int_{-\infty}^{+\infty}\frac{\widetilde{S}(K_z)\widetilde{\Psi}_{\text{inc}}(n_0k_x-K_x)}{Z(n_0k_x)}I_1^-(K_z,n_0k_x,L_+)dK_z + \left(\frac{k^2n_0\hat{n}}{2}\right)^3 \int_{-\infty}^{+\infty}\int_{-\infty}^{+\infty}\int_{-\infty}^{+\infty}$$

$$\times\left(\frac{\widetilde{S}^*(K_z)\widetilde{S}(K_z')\widetilde{S}(K_z'')\widetilde{\Psi}_{\text{inc}}(n_0k_x+K_x-K_x'-K_x'')}{Z(n_0k_x)Z(n_0k_x+K_x)Z(n_0k_x+K_x-K_x')}I_3^{+--}(K_z,K_z',K_z'',n_0k_x,L_+)\right.$$

$$+\frac{\widetilde{S}(K_z)\widetilde{S}^*(K_z')\widetilde{S}(K_z'')\widetilde{\Psi}_{\text{inc}}(n_0k_x-K_x+K_x'-K_x'')}{Z(n_0k_x)Z(n_0k_x-K_x)Z(n_0k_x-K_x+K_x')}I_3^{-+-}(K_z,K_z',K_z'',n_0k_x,L_+)$$

$$+\left.\frac{\widetilde{S}(K_z)\widetilde{S}(K_z')\widetilde{S}^*(K_z'')\widetilde{\Psi}_{\text{inc}}(n_0k_x-K_x-K_x'+K_x'')}{Z(n_0k_x)Z(n_0k_x-K_x)Z(n_0k_x-K_x-K_x')}I_3^{--+}(K_z,K_z',K_z'',n_0k_x,L_+)\right)dK_z''\,dK_z'\,dK_z, \tag{11}$$

with

$$I_3^{---}(K_z,K_z',K_z'',n_0k_x,L_+) = \int_{L_-}^{L_+} e^{-iz'A(K_z,n_0k_x)}\int_{L_-}^{z'} e^{-iz''A(K_z',n_0k_x-K_x)}\int_{L_-}^{z''} e^{-iz'''A(K_z'',n_0k_x-K_x-K_x')}\,dz'''\,dz''\,dz',$$

$$I_3^{+--}(K_z,K_z',K_z'',n_0k_x,L_+) = \int_{L_-}^{L_+} e^{iz'B(K_z,n_0k_x)}\int_{L_-}^{z'} e^{-iz''A(K_z',n_0k_x+K_x)}\int_{L_-}^{z''} e^{-iz'''A(K_z'',n_0k_x+K_x-K_x')}\,dz'''\,dz''\,dz',$$

$$I_3^{-+-}(K_z,K_z',K_z'',n_0k_x,L_+) = \int_{L_-}^{L_+} e^{-iz'A(K_z,n_0k_x)}\int_{L_-}^{z'} e^{iz''B(K_z',n_0k_x-K_x)}\int_{L_-}^{z''} e^{-iz'''A(K_z'',n_0k_x-K_x+K_x')}\,dz'''\,dz''\,dz',$$

and

$$I_3^{--+}(K_z,K_z',K_z'',n_0k_x,L_+) = \int_{L_-}^{L_+} e^{-iz'A(K_z,n_0k_x)} \int_{L_-}^{z'} e^{-iz''A(K_z',n_0k_x-K_x)} \int_{L_-}^{z''} e^{iz'''B(K_z',n_0k_x-K_x-K_x')} \, dz''' \, dz'' \, dz'.$$

The next step would be to find an expression for the fourth-order diffraction decompositions together with a correction for the second and zeroth orders based on Eqs. (10) and (11). Continuing this procedure of consecutive backsubstitution for a while, it is obvious that one can write the general expression for the spectral decomposition of any diffraction order as a series expansion in which the consecutive terms contain more and more complicated integral expressions. Supposing m is positive, the rth term in the expression for the Fourier transformation of the mth diffraction order is a $2(2r-2+m)$-multiple integral over

$$\binom{2r-2+m}{r-1}$$

terms, which corresponds exactly to the number of possible ways in which one can reach the mth diffraction order, starting from the zeroth order, in a $(2r-2+m)$ combination of $(r-1+m)$ elementary upshifted and $(r-1)$ elementary downshifted diffractions. This leads to the same idea as used in the Feynman diagram approach of Korpel and Poon.[15–17]

The deduction presented here, is based on the results obtained by means of a backsubstitution method of Aggarwal[22] for the case of the interaction between infinite plane waves. It is straightforward to check that his expressions for the diffracted light intensities coincide with our results in the case when both light and sound spectral distributions are represented by a delta function.

C. Symmetry properties of the diffraction orders

Before analyzing the Fourier-transformed amplitudes and calculating the light distribution in the diffracted orders, it is instructive to note some symmetry properties which can be deduced from the general series expansion. If $n_0 k_{inc_x} = n_0 k \sin \varphi_{inc}$ defines the incidence angle of the light beam in the liquid with respect to the z axis, normal to the propagation direction of the sound beam (which we suppose to be parallel to the x axis), we find that
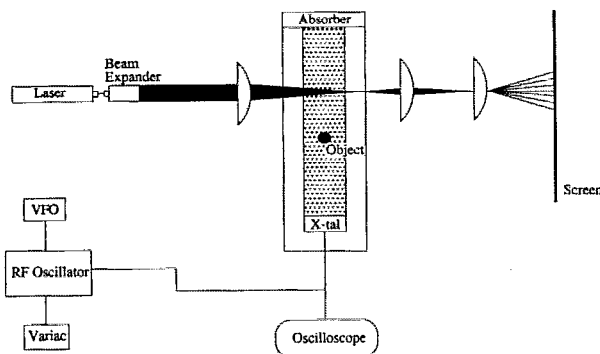
$$\tilde{\Psi}_m(n_0k_x,z)\big|_{inc=n_0k_{inc_x}}$$
$$= (-1)^m \tilde{\Psi}_{-m}(-n_0k_x,z)\big|_{inc=-n_0k_{inc_x}}, \tag{12a}$$

if

$$\tilde{S}(K_z) = \tilde{S}^*(-K_z)$$

and

$$\tilde{\Psi}_{inc}(n_0k_x)\big|_{inc=n_0k_{inc_x}}$$
$$= \tilde{\Psi}_{inc}(-n_0k_x)\big|_{inc=-n_0k_{inc_x}}. \tag{12b}$$

As a consequence, this means that the angular spectra of the mth and $-m$th diffraction order in the case of perpendicularity between the main propagation directions of light and sound are mirror distributions with respect to the normal axis if the incident light beam has a symmetric spectrum with respect to this normal axis and if there is no phase variation in the sound beam profile along the interaction region (L_-,L_+) at $x=x_0$. Besides, substituting Eq. (12a) in Eq. (4b), it can be shown that, under these specific circumstances given in Eq. (12b), the field distributions in opposite orders are mirrored with respect to $x=x_0$, i.e.,

$$\Psi_m(\xi,z) = (-1)^m \Psi_{-m}(-\xi,z). \tag{12c}$$

In terms of experimental observations, this symmetry property explains why the images in the positive orders show up like mirror images of those in the corresponding negative orders. In the experimental arrangement, as diagramed in Fig. 3, first Martin[20] and later Na[21] use a collimated laser beam which is first expanded. Then a cylindrical lens is used to converge the light to make a wedge of light symmetrical with respect to the normal axis. By placing a wire hook in the ultrasonic field, one obtains images as well in the positive as in the corresponding negative diffraction orders at the same time. Figure 4, made by Na,[21] shows that mirror images of the hook appear in both plus and minus first diffraction orders as is expected from the symmetry properties of Eq. (12c).
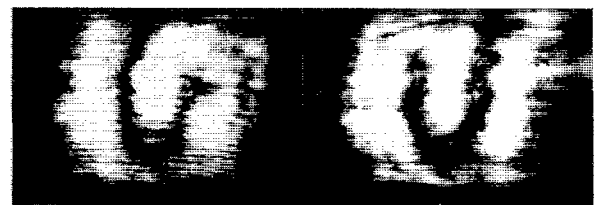
FIG. 3. Experimental setup for a multiple Bragg imaging system.

FIG. 4. Photographs of positive and negative first-order Bragg images of a hook at a frequency of 20 MHz (Ref. 21).

Van Den Abeele et al.

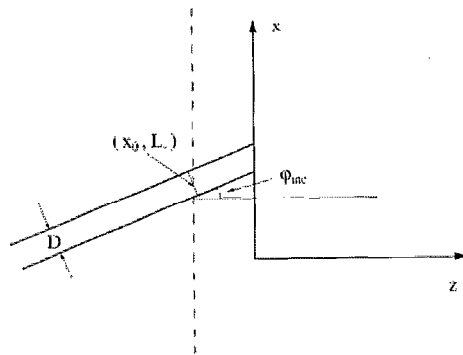FIG. 5. Representation of a thin uniform light beam at incidence angle φ_{inc}.

FIG. 6. Schematic visualization of the mth-order diffraction of a thin light beam incident at $\varphi_{\text{inc}} = -m\varphi_B$.

D. Imaging in the higher orders

1. General considerations

In order to obtain evidence for the appearance of multiple images in the higher Bragg diffraction orders when using a light beam with considerable convergence angle, we focus our attention on the first term in the series expansion for the spectral decomposition of the diffaction orders. The reason for this is not only because we can already distinguish that the first term for the first diffraction order contains single information about the sound beam [Eq. (7)], for the second diffracted order two-fold information [Eq. (8)] and for the third-order three-fold information [Eq. (10)], but also because careful analysis of the general expression reveals that the higher-order terms are proportional to higher powers of the Raman–Nath parameter $[v = k\hat{n}(L_+ - L_-)]$ and/or higher powers of the parameter $1/\rho$ ($= n_0 \hat{n} k^2/K^2$). This restriction thus means that we are working with low-power ultrasound in a high-frequency range. In addition we suppose that the convergent light beam can be represented by a number of thin light rays with equal amplitude and frequency but incident at slightly different angles. The angular spectrum of a beam of light with uniform amplitude A_0 over a finite width D, centered at the point (x_0, L_-) and having a direction defined by $n_0 k_{\text{inc}_x} = n_0 k \sin \varphi_{\text{inc}}$ (see Fig. 5), is given by
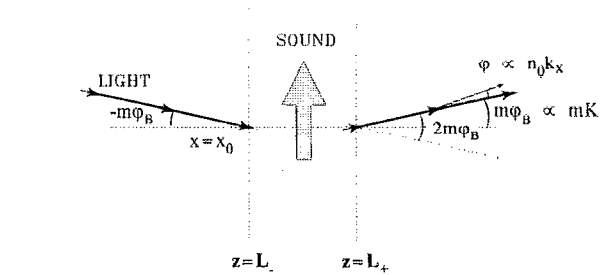
$$\widetilde{\Psi}_{\text{inc}}(n_0 k_x) = \frac{A_0 D}{2\pi \cos \varphi_{\text{inc}}}$$

$$\times \frac{\sin\{[n_0 D(k_x - k_{\text{inc}_x})/2 \cos \varphi_{\text{inc}}]\}}{[n_0 D(k_x - k_{\text{inc}_x})/2 \cos \varphi_{\text{inc}}]} e^{in_0 k_z L_-}. \tag{13}$$

Letting D go to zero, while $A_0 D$ remains finite, we find for the Fourier spectrum of the infinitely small ray through (x_0, L_-) in the direction φ_{inc}

$$\widetilde{\Psi}_{\text{inc}}(n_0 k_x) = \frac{A_0 D n_0 k}{2\pi Z(n_0 k_{\text{inc}_x})} e^{in_0 k_z L_-}. \tag{14}$$

For plane-wave interactions it is known that the mth diffraction order intensity has an extremum for an incidence angle φ_{inc} equal to $-m\varphi_B$, when φ_B is the Bragg angle[2]

$$\frac{\lambda}{2n_0 \Lambda} = \frac{K}{2n_0 k}. \tag{15}$$

Therefore, we are especially interested in the spectral distribution of the mth diffraction order generated when a thin light beam is incident at the minus mth Bragg angle, i.e., when $n_0 k_{\text{inc}_x} = -m(K/2)$ (see Fig. 6). Assuming only weak divergence of the sound beam [such that we can approximate $Z(s + K - K_x)$ by $Z(s)$], we obtain the following expression for the first term in the series expansion for the mth diffracted order:

$$\widetilde{\Psi}_m\left(n_0 k_x + \frac{m}{2} K, L_+\right) = \left(-\frac{k^2 n_0 \hat{n}}{2}\right)^m \frac{A_0 D n_0 k}{2\pi Z[-(m/2)K]} \frac{e^{iZ[n_0 k_x - (m/2)K]L_-}}{\Pi_{j=1}^m Z\{n_0 k_x + [j - (m/2)]K\}} H_m(n_0 k_x, L_+), \tag{16}$$

with

$$H_r(n_0 k_x, z) = \int_{L_-}^{z} S(0, z') \exp\left[iKz'\left(\frac{Z\{n_0 k_x + [r - (m/2)]K\} - Z\{n_0 k_x + [r - 1 - (m/2)]K\}}{K}\right)\right] H_{r-1}(n_0 k_x, z') dz'$$

and

$$H_0(n_0 k_x, z) = 1.$$

[We restrict ourselves to cases where m is a positive integer, but the results for negative values of m are analogous because of the symmetry properties given in Eq. (12).]

In Eq. (16) $n_0 k_x$ corresponds to the spectral variation with respect to $(m/2)K$, which is equivalent to the angular variation φ around the mth Bragg angle with respect to the normal behind the interaction vessel (see Fig. 6).

The two-dimensional field of the mth diffraction order at $z = L_+$ can be calculated from Eqs. (16) and (4b), which leads to the following approximation for the mth diffracted amplitude distribution at the exit plane:

$$\Psi_m(\xi, L_+) = \left(-\frac{k^2 n_0 \hat{n}}{2}\right)^m \frac{A_0 D n_0 k}{2\pi Z[-(m/2)K]} \int_{-\infty}^{+\infty} \frac{H_m(n_0 k_x, L_+)}{\Pi_{j=1}^m Z\{n_0 k_x + [j - (m/2)]K\}}$$

$$\times e^{-i\{Z[n_0 k_x + (m/2)K]L_+ - Z[n_0 k_x - (m/2)K]L_-\}} e^{-i[n_0 k_x + (m/2)K]\xi} \, dn_0 \, k_x. \tag{17}$$

From Eqs. (16) and (17) one can write down the expressions for the spectral decomposition and the field distribution for the orders $m = 1, 2$ and 3.

2. First order $m = 1$

Writing Eq. (16) explicitly for $m = 1$ yields

$$\tilde{\Psi}_1(n_0 k_x + (K/2), L_+) = -\frac{k^2 n_0 \hat{n}}{2} \frac{A_0 D n_0 k}{2\pi Z(-K/2)} \frac{e^{iZ[n_0 k_x - (K/2)]L_-}}{Z[n_0 k_x + (K/2)]}$$

$$\times \int_{L_-}^{L_+} S(0, z') \exp\left[iKz'\left(\frac{Z(n_0 k_x + (K/2)) - Z[n_0 k_x - (K/2)]}{K}\right)\right] dz'. \tag{18}$$

Substituting the second-order approximation

$$\frac{Z[n_0 k_x + r(K/2)] - Z[n_0 k_x + (r-2)(K/2)]}{K}$$

$$\approx -\left(\frac{n_0 k_x + (r-1)(K/2)}{n_0 k_x}\right) \approx -\sin[\varphi + (r-1)\varphi_B] \tag{19}$$

for $r = 1$ in Eq. (18) and recalling Eq. (3b), we find that

$$\tilde{\Psi}_1\left(n_0 k_x + \frac{K}{2}, L_+\right) Z\left(n_0 k_x + \frac{K}{2}\right)$$

$$\approx -2\pi \frac{k^2 n_0 \hat{n}}{2} \frac{A_0 D n_0 k}{2\pi Z(-K/2)} e^{iZ[n_0 k_x - (K/2)]L_-}$$

$$\times \tilde{S}\left(-K\frac{n_0 k_x}{n_0 k}\right), \tag{20}$$

which can formally be rewritten as follows:

$$\tilde{\Psi}_1\left(n_0 k_x + \frac{K}{2}, L_+\right) \approx \text{Cte } \tilde{\Psi}_{\text{inc}}\left(n_0 k_x - \frac{K}{2}\right) \tilde{S}\left(-K\frac{n_0 k_x}{n_0 k}\right), \tag{21}$$

or in terms of angles as

$$\tilde{\Psi}_1[n_0 k \sin(\varphi + \varphi_B), L_+]$$

$$\approx \text{Cte } \tilde{\Psi}_{\text{inc}}[n_0 k \sin(\varphi - \varphi_B)] \tilde{S}(-K \sin \varphi). \tag{22}$$

This result confirms the parametric mixing theory used by Korpel[14] to prove that the first-order diffraction intensity of a small uniform light beam has the same spectral decomposition as the sound beam when Bragg conditions occur, i.e., when the angle of incidence is equal to the minus first Bragg angle. The approach used to derive Eq. (22) has the advantage that all approximations needed in the derivation are explicitly stated.

The field distribution in the first diffraction order at the exit plane $z = L_+$ then becomes an image of the sound beam profile at the interaction cross-section $x = x_0$,

$$\Psi_1(\xi, L_+) \approx -\frac{A_0 D k^3 n_0^2 \hat{n}}{4KZ(-K/2)} \exp\{-in_0 k[(L_+ - L_-)$$

$$\times \cos \varphi_B + \xi \varphi_B]\}$$

$$\times S\left(0, \frac{n_0 k}{K}[-\xi + (L_+ + L_-)\varphi_B]\right). \tag{23}$$

Equation (23), which is the mapping function derived by Korpel, clearly illustrates the one-to-one mapping of the ultrasonic field onto the first diffraction order and exhibits the corresponding imaging rules. There is a projection of the z coordinate along the interaction region inside the sound field at $x = x_0$ onto the ξ coordinate in the observation plane at $z = L_+$ (see Fig. 7). The minus sign indicates a mapping of $-z$ onto $+\xi$, while the factor $K/n_0 k = 2\varphi_B$ accounts for the demagnification of the image of the sound
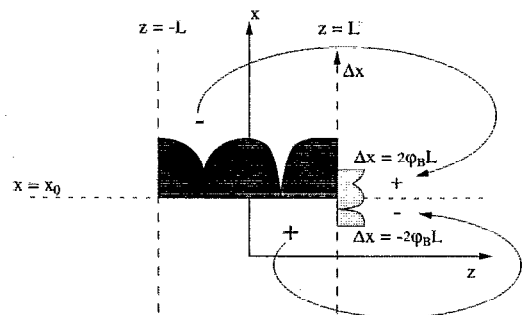

FIG. 7. Mapping rules in the positive first diffraction order $(L_+ = -L_- = L)$.

Van Den Abeele et al.

field proportional to the ratio of the frequencies of the ultrasonic wave and the light wave. $(L_+ - L_-)$ represents the acousto-optic interaction length, while the term $(L_+ + L_-)\varphi_B$ in the sound field function S takes into account the position of the sound beam with respect to the theoretical origin $z=0$, so that the optical image is always centered around $\xi=0$.

Although Eq. (23) predicts an exact image independent of frequency and width of the ultrasonic beam, this deduction is valid only for situations in which rather "extreme Bragg conditions" occur, i.e., high frequencies and weak sound beam divergence (or large interaction width). Whenever these conditions are only partially fulfilled, the approximation should be modified and additional terms [in this case the second term in Eq. (11), which is a triple integral] in the series expansion must be taken into account. Experimentally it is observed that the quality of the first diffraction order images of small objects positioned in the ultrasonic field between the transducer and the light beam improves with increasing ultrasonic frequency, with the best images occurring for 18 MHz and above.[20,21]

Note that in this approximation the relative intensity of the first diffraction order, focused to a point by a lens system, for the case of a uniform sound field of width $2L$, becomes

$$\frac{I_1}{I_{\text{total}}} = \frac{v^2}{4}, \tag{24}$$

with v the Raman–Nath parameter $k\hat{n}2L$. This result is in agreement with the Aggarwal solution[22] and corresponds to the first term in the Phariseau solution for exact Bragg conditions in the interaction of plane uniform sound and light beams.[25]

The same approximations needed to obtain Eqs. (20) and (23) can be used in an analogous way to deduce the expressions for higher diffraction orders. We suppose for simplification that $L_+ = -L_- = L$.

3. Second order m=2

The expression for the spectral decomposition of the second diffraction order for a small uniform light beam incident at the minus second Bragg angle becomes

$$\tilde{\Psi}_2(n_0 k_x + K, L)Z(n_0 k_x + K) = \frac{4\pi^2}{Z(n_0 k_x)}\left(\frac{k^2 n_0 \hat{n}}{2}\right)^2 \frac{A_0 D n_0 k}{2\pi Z(-K)} \exp\left[-iZ(n_0 k_x - K)L\right]\frac{1}{2\pi}\frac{1}{2\pi}\int_{-L}^{L} S(0,z')$$

$$\times \exp\left[-iKz'\left(\frac{n_0 k_x + (K/2)}{n_0 k}\right)\right]\int_{-L}^{z'} S(0,z'')\exp\left[-iKz''\left(\frac{n_0 k_x - (K/2)}{n_0 k}\right)\right]dz''\,dz', \tag{25}$$

and the field distribution can be approximated by

$$\Psi_2(\xi,L) \approx \frac{A_0 D k^4 n_0^2 \hat{n}^2}{4KZ(-K)} \exp\left[-in_0 k(2L\cos 2\varphi_B + \xi 2\varphi_B)\right]\exp\left(-in_0 k 2\varphi_B^2 \frac{\xi}{2\varphi_B}\right)$$

$$\times \int_{-L}^{L} S(0,z_1)S\left(0,-z_1-\frac{\xi}{2\varphi_B}\right)\text{Int}_{\xi/2\varphi_B}[-2z_1,L-z_1]e^{-in_0 k 4\varphi_B^2 z_1}\,dz_1, \tag{26}$$

with $\text{Int}_s[a,b]$ the interval function defined as the difference of two Heaviside functions so that

$$\text{Int}_s[a,b] = 1 \quad \text{if } a \leqslant s \leqslant b, \tag{27}$$

$$\text{Int}_s[a,b] = 0 \quad \text{everywhere else.}$$

Introducing the Klein–Cook–Mayer parameter[1] for a uniform plane sound wave of width $2L$,

$$Q = 2\varphi_B K(2L) = vp, \tag{28}$$

and combining partial integration with rules for calculating the derivatives of Heaviside functions,[26] we find that

$$\Psi_2(\xi,L) \approx \frac{A_0 D k^4 n_0^2 \hat{n}^2}{4KZ(-K)} \exp[-in_0 k(2L\cos 2\varphi_B + \xi 2\varphi_B)] \tag{29}$$

$$\times \left\{ -i\frac{2L}{Q} S\left(0,-\frac{\xi}{4\varphi_B}\right) S\left(0,-\frac{\xi}{4\varphi_B}\right) \mathrm{Int}_\xi[-2\varphi_B(2L),2\varphi_B(2L)] \right. \tag{A}$$

$$+i\frac{2L}{Q} S(0,-L)S\left(0,L-\frac{\xi}{2\varphi_B}\right)\exp\left[-i\frac{Q}{4L}\left(2L-\frac{\xi}{2\varphi_B}\right)\right]\mathrm{Int}_\xi[0,2\varphi_B(2L)] \tag{B}$$

$$+i\frac{2L}{Q} S(0,L)S\left(0,-L-\frac{\xi}{2\varphi_B}\right)\exp\left[-i\frac{Q}{4L}\left(2L+\frac{\xi}{2\varphi_B}\right)\right]\mathrm{Int}_\xi[-2\varphi_B(2L),0] \tag{C}$$

$$\left. -i\frac{2L}{Q}\int_{-L}^{L} \frac{\partial\{S(0,z_1)S[0,-(\xi/2\varphi_B)-z_1]\}}{\partial z_1}\exp\left[-i\frac{Q}{4L}\left(2z_1+\frac{\xi}{2\varphi_B}\right)\right]\mathrm{Int}_{\xi/2\varphi_B}[-2z_1,L-z_1]dz_1 \right\}. \tag{D}$$

Again, one can verify that these results match the Aggarwal results for uniform plane-wave interaction by assuming $S(0,z)$ equal to unity over the interval $(-L,L)$, and integrating along the ξ axis in the exit plane over $(-4\varphi_B L, 4\varphi_B L)$.

Term (A) in Eq. (29) indicates that the second-order field distribution at the exit plane consists of a large image of the sound field in the second power which extends over the range $(-4\varphi_B L, 4\varphi_B L)$. On the other hand, terms (B) and (C) represent two images of the sound beam with the same dimensions as the image in the first diffraction order, i.e., $4\varphi_B L$. One of them is upshifted and the other downshifted with respect to the center $\xi=0$ over a distance $2\varphi_B L$. The result is that these images are adjoining and that their center-to-center separation at the exit plane is equal to $4\varphi_B L$. Further use of partial integration proves that the fourth term (D) corresponds to a second-order effect in $2L/Q$ for sufficiently high ultrasonic frequencies and in the assumption that S^2 and its derivatives are slowly varying functions. Seeing the incorporation of an object as shadows in a uniform (amplitude equal to unity) sound field which extends from $-L$ to L and neglecting all second- and higher-order terms in $2L/Q$, we find theoretical evidence for the presence of two adjoining images of the sound beam in the second diffraction order, as shown for an experimental example in Fig. 8 (Na[21]). From a

theoretical point of view, one can explain the fact that the images in the second diffraction order are less distinct because the additional terms also can play a role in the blurring of the field distribution. In the first place, term (A) would appear as an enlarged image superimposed on the adjacent images (although it does not show up in the experimental examples) and for lower frequencies term (D) has to be taken into account along with additional terms in the series expansion for the spectral decomposition of the second diffraction order. Important for the imaging is the phase factor in terms (B) and (C) of Eq. (29) which is determined by the value of Q. Analyzing the intensity distribution in the case of a uniform sound field of width $2L$, one can expect theoretically that the best reproduction of the two adjoining images occurs for a value of Q equal to 4π. Figure 9 compares the second orders for a small light

FIG. 8. First- and second-order diffraction fields of an ultrasonic beam containing the shadows of a nut at a frequency of 12 MHz (Ref. 21).
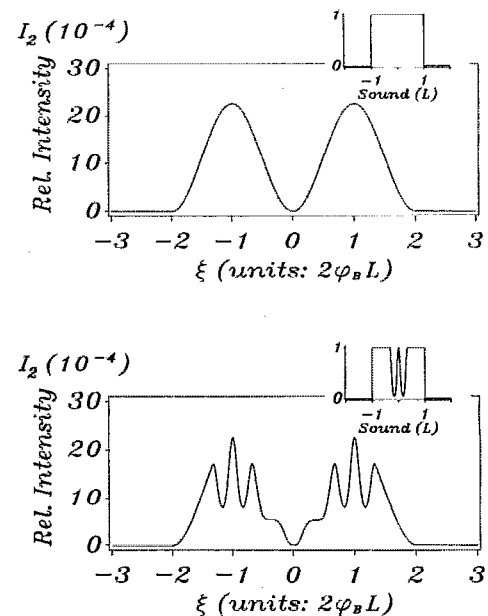

FIG. 9. Theoretical calculations of the second-order diffracted field intensity of a uniform and a shadow containing ultrasonic field according to the first three terms in Eq. (29) relative to the maximum of the first diffraction order intensity ($Q=4\pi$, $L=3$ cm).

Van Den Abeele et al.

beam incident at $-2\varphi_B$ which is diffracted by a uniform and a shadow-containing sound field, at this specific value.

As a system of lenses is used in experiments to view each order on a screen, the above theoretical deduction predicts that the center-to-center separation of the two adjoining images within the second diffraction order is proportional to the width of the ultrasonic beam and to its frequency. Experiments performed by Na[21] for different ultrasonic frequencies and beam widths confirm this pre-

dicted linear dependence of the center-to-center separation on F and L as is shown in Fig. 10.

4. Third order m = 3

For the third diffraction order of a small uniform light beam incident at the minus third Bragg angle, we use the same approximations and find the following expression for the spectral decomposition:

$$
\widetilde{\Psi}_3\left(n_0k_x+3\frac{K}{2},L\right)Z\left(n_0k_x+3\frac{K}{2}\right)= -\frac{8\pi^3}{Z[n_0k_x-(K/2)]Z[n_0k_x+(K/2)]}\left(\frac{k^2n_0\hat{n}}{2}\right)^3\times\frac{A_0Dn_0k}{2\pi Z(-\tfrac{3}{2}K)}\exp\{-iZ[n_0k_x
$$

$$
-3(K/2)]L\}\frac{1}{2\pi}\frac{1}{2\pi}\frac{1}{2\pi}\int_{-L}^{L}S(0,z')\exp\left[-iKz'\left(\frac{n_0k_x+K}{n_0k}\right)\right]\int_{-L}^{z'}S(0,z'')
$$

$$
\times\exp\left[-iKz''\left(\frac{n_0k_x}{n_0k}\right)\right]\int_{-L}^{z''}S(0,z''')\exp\left[-iKz'''\left(\frac{n_0k_x-K}{n_0k}\right)\right]dz'''\,dz''\,dz'. \tag{30}
$$

Subsequently, the field distribution becomes

$$
\Psi_3(\xi,L)\approx -\frac{A_0Dk^5n_0^2\hat{n}^3}{8KZ[-3(K/2)]}\exp[-in_0k(2L\cos3\varphi_B+\xi3\varphi_B)]\exp\left(-in_0k4\varphi_B^2\frac{\xi}{2\varphi_B}\right)\int_{-L}^{L}S(0,z_2)e^{-in_0k8\varphi_B^2z_2}
$$

$$
\times\int_{-L}^{z_2}S(0,z_1)S\left(0,-z_1-z_2-\frac{\xi}{2\varphi_B}\right)\mathrm{Int}_{\xi/2\varphi_B}[-2z_1-z_2,L-z_2-z_1]e^{-in_0k4\varphi_B^2z_1}\,dz_1\,dz_2. \tag{31}
$$

Calculating the leading terms also in this case, we obtain

$$
\Psi_3(\xi,L)\approx -\frac{A_0Dk^5n_0^2\hat{n}^3}{8KZ[-3(K/2)]}\exp[-in_0k(2L\cos3\varphi_B+\xi3\varphi_B)] \tag{32}
$$

$$
\times\left\{-\frac{4}{3}\frac{L^2}{Q^2}S\left(0,-\frac{\xi}{6\varphi_B}\right)S\left(0,-\frac{\xi}{6\varphi_B}\right)S\left(0,-\frac{\xi}{6\varphi_B}\right)\mathrm{Int}_\xi[-2\varphi_B(3L),2\varphi_B(3L)]\right. \tag{A}
$$

$$
+\frac{8}{3}\frac{L^2}{Q^2}S(0,-L)S\left(0,\frac{L}{2}-\frac{\xi}{4\varphi_B}\right)S\left(0,\frac{L}{2}-\frac{\xi}{4\varphi_B}\right)\exp\left[-i\frac{Q}{4L}\left(3L-\frac{\xi}{2\varphi_B}\right)\right]\mathrm{Int}_\xi[-2\varphi_BL,2\varphi_B(3L)] \tag{B}
$$

$$
+\frac{8}{3}\frac{L^2}{Q^2}S(0,L)S\left(0,-\frac{L}{2}-\frac{\xi}{4\varphi_B}\right)S\left(0,-\frac{L}{2}-\frac{\xi}{4\varphi_B}\right)\exp\left[-i\frac{Q}{4L}\left(3L+\frac{\xi}{2\varphi_B}\right)\right]\mathrm{Int}_\xi[-2\varphi_B(3L),2\varphi_BL] \tag{C}
$$

$$
-\frac{4}{3}\frac{L^2}{Q^2}S(0,-L)S(0,-L)S\left(0,2L-\frac{\xi}{2\varphi_B}\right)\exp\left[-i\frac{Q}{4L}\left(6L-\frac{\xi}{\varphi_B}\right)\right]\mathrm{Int}_\xi[2\varphi_BL,2\varphi_B(3L)] \tag{D}
$$

$$
-4\frac{L^2}{Q^2}S(0,-L)S(0,L)S\left(0,-\frac{\xi}{2\varphi_B}\right)\exp[-iQ]\mathrm{Int}_\xi[-2\varphi_BL,2\varphi_BL] \tag{E}
$$

$$
-\frac{4}{3}\frac{L^2}{Q^2}S(0,L)S(0,L)S\left(0,-2L-\frac{\xi}{2\varphi_B}\right)\exp\left[-i\frac{Q}{4L}\left(6L+\frac{\xi}{\varphi_B}\right)\right]\mathrm{Int}_\xi[-2\varphi_B(3L),-2\varphi_BL] \tag{F}
$$

$$
\left.+\cdots\text{ third- and higher-order terms in }\frac{2L}{Q}\right\}.
$$

In this third-order diffraction field, we can distinguish a triple-enlarged (compared to the image in the first diffraction order) cubic power of the sound image over the interval $(-6\varphi_BL,6\varphi_BL)$ (A), two double-enlarged images in the second power centered at $\xi=\pm2\varphi_BL$ [(B) and

(C)], and three adjoining images [(D), (E), and (F)] of the same dimensions as the first diffraction order image with a center-to-center separation equal to $4\varphi_BL$. As a consequence, the field distribution in the third diffraction order of a small light beam incident at $-3\varphi_B$, diffracted by

a uniform field in which an object is incorporated in the form of a shadow, will contain information about this object in the form of three adjacent images, once centered, once shifted in positive ξ direction by $4\varphi_B L$, and once in negative direction shifted over the same distance. As in the case for the second diffraction order, additional terms cause blurring and reduce the quality of the three images. An experimental example of this triple imaging is shown in Fig. 1, while Fig. 11 illustrates the effect of a shadow in a uniform sound field on the third diffraction order for the same parameters as in Fig. 9. The theory predicts the intensity of the image in the center lobe to be four times as large as the shifted images. Analyzing the phase terms in Eq. (32) and reasoning analogously as in the case of a uniform sound beam, one finds again that the best imaging can be obtained for Q equal to 4π.

5. Arbitrary order m

In general, for a thin light beam incident at the angle $-m\varphi_B$, Eq. (17) for the mth-order diffraction field $(m \geqslant 1)$ can also be written in the following form which suggests a cumulative effect:

$$\Psi_m(\xi,L) \approx (-1)^m \frac{A_0 D k^{m+2} n_0^2 \hat{n}^m}{2^m K Z[-m(K/2)]}$$
$$\times \exp[-in_0 k(2L\cos m\varphi_B + m\varphi_B \xi)]$$
$$\times F_m\left(\frac{\xi}{2\varphi_B}, z_m = L\right), \qquad (33)$$

with

$$F_r(s,z_r) = \int_{-L}^{z_r} S(0,z_{r-1}) e^{-in_0 k2(r-1)\varphi_B^2 z_{r-1}}$$
$$\times F_{r-1}(-z_{r-1}-s, z_{r-1}) e^{in_0 k2\varphi_B^2(-z_{r-1}-s)} dz_{r-1}$$

and

$$F_0(s,z_0) = \delta(-s).$$

Retaining only the predominant terms in this expression, we obtain:

$$\Psi_m(\xi,L) \approx (-1)^m \frac{A_0 D k^{m+2} n_0^2 \hat{n}^m}{2^m K Z[-m(K/2)]} \exp[-in_0 k(2L\cos m\varphi_B + m\varphi_B \xi)] \left(4i\frac{L}{Q}\right)^{m-1} \sum_{k=1}^{m} \sum_{l=1}^{m-k+1} A_{k,l}^{(m)}$$
$$\times [S(0,-L)]^{l-1} \left[S\left(0, \frac{(-m+k+2l-2)}{k}L - \frac{\xi}{2k\varphi_B}\right) \right]^k [S(0,L)]^{m-k-l+1} \times \exp\left\{ -\frac{iQ}{4L}\left[2(m-k-l+1)\right.\right.$$
$$\left.\left. \times (m-l+1)L - (m-k-2l+2)\left(mL-\frac{\xi}{2\varphi_B}\right)\right] \right\} \mathrm{Int}_{\xi/2\varphi_B}[-(m-2l+2)L, -(m-2k-2l+2)L], \qquad (34)$$
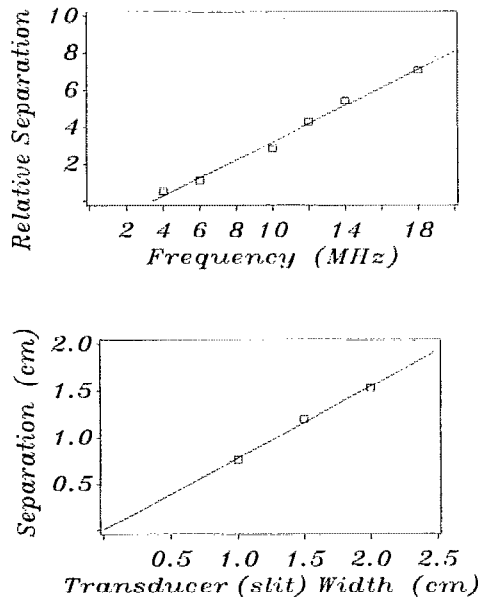

FIG. 10. Experimental confirmation of the linear dependence of the center-to-center separation of the double images in the second diffraction order on ultrasonic frequency and beam width.
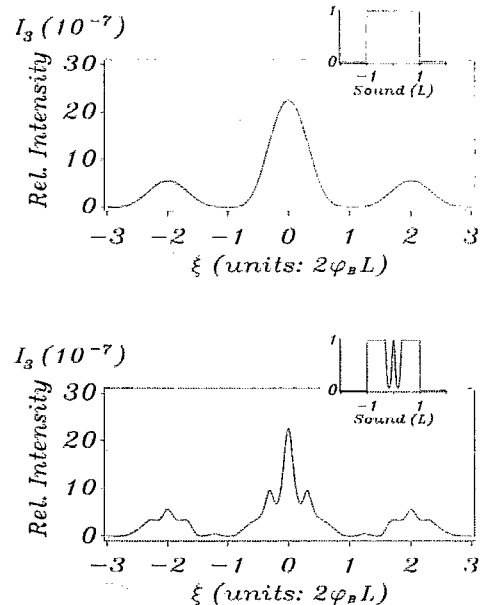

FIG. 11. Theoretical calculations of the third-order diffracted field intensity of a uniform and a shadow containing ultrasonic field according to the first six terms in Eq. (32) relative to the maximum of the first diffraction order intensity ($Q=4\pi$, $L=3$ cm).

where the coefficients $A_{k,l}^{(m)}$ can be calculated from the following recurrence relation:

$$A_{k,l}^{(m)} = \frac{A_{k,l}^{(m-1)}}{(m-l+1)(m-k-l+1)} \quad \text{if } k+l \leqslant m, \qquad (35a)$$

$$A_{k,l}^{(m)} = \sum_{j=1}^{l-1} A_{j,l-j}^{(m)} - \sum_{j=1}^{k-1} A_{j,l}^{(m)} \quad \text{if } k+l=m+1, \qquad (35b)$$

and

$$A_{1,1}^{(1)} = 1. \qquad (35c)$$

The terms with $k=1$ indicate that m adjoining images of the sound cross section contribute to the field distribution in the mth diffracted order. These images are demagnified by a factor $2\varphi_B$ compared to the real sound field and the distance from center to center is equal to $4\varphi_B L$.

E. Using a convergent lightbeam

As a first approximation, we may imagine a number of thin uniform light rays, incident at different angles, as a rudimentary model for a convergent light beam. The aggregation of the diffraction extrema for all those rays incident at specific Bragg angles then explains the simultaneous observation of a single image in the first diffraction orders and multiple adjoining images in the higher diffraction orders as was reported by Martin and co-workers.[20] If the convergent beam is symmetric with respect to the normal axis, the images in positive orders are mirror images of the negative diffraction orders due to the symmetry property given in Eq. (12). We note that the angular aperture of the symmetrically incident convergent beam must be larger than $2m$ Bragg angles in order to generate a positive and negative m-multiple image for a well-chosen frequency-width combination of the sound field. The theoretically predicted proportionality of the leading terms in the mth diffraction order to $(L/Q)^m$ [Eq. (34)] indicates that the higher-order images can be observed only by lowering the ultrasonic frequencies. Subsequently, the quality of the lower diffraction order images becomes poorer when higher-order images are observed. The blurring of these lower diffraction order images at smaller Q/L values means that, from a theoretical point of view, additional terms in the series expansion of their field distributions should be taken into account.

III. CONCLUSIONS

Using Fourier analysis and a backsubstitution method, we derived general expressions for the angular spectrum of the diffracted orders of profiled light after interaction with profiled sound waves. We found that the first term in the series expansions for the spectral distribution of mth diffracted field contains $|m|$-fold information about the sound profile. Recalling that the mth diffraction order intensity is maximal for light waves incident at $-m$ times the Bragg angle and limiting ourselves to this first term in the series expansions we could obtain theoretical evidence for the simultaneous appearance of multiple images in the higher diffraction orders when a convergent light beam is illuminating a sound field in Bragg conditions. This theory also explains the mirror effect for positive and negative diffraction orders and its basic ideas predict a linear dependence of the center-to-center separation of the images within the higher diffraction orders on the ultrasonic frequency and beam width as has been experimentally verified.

[1] W. R. Klein, B. D. Cook, and W. G. Mayer, Acustica 15, 67 (1965).
[2] E. Blomme and O. Leroy, Acustica 63, 83 (1987).
[3] K. Van Den Abeele and O. Leroy, J. Acoust. Soc. Am. 88, 2298 (1990).
[4] O. Leroy and R. Mertens, Acustica 26, 96 (1972).
[5] J. C. Berlinghieri and B. D. Cook, J. Acoust. Soc. Am. 58, 823 (1975).
[6] B. D. Cook and J. C. Berlinghieri, J. Acoust. Soc. Am. 61, 1477 (1977).
[7] R. Reibold and W. Molkenstruck, Acustica 56, 181 (1984).
[8] R. Reibold and W. Molkenstruck, in Proceedings FASE 84, Sandefjord, Norway 1984, edited by J. Tro, pp. 81–84.
[9] P. Kwiek and R. Reibold, Acustica 71, 69 (1990).
[10] E. Blomme, P. Kwiek, O. Leroy, and R. Reibold, Acustica 73, 134 (1991).
[11] S. N. Antonov, V. N. Sotnikov, O. Leroy, and K. Van Den Abeele, Ultrasonics 29, 366 (1991).
[12] K. Van Den Abeele and O. Leroy, Ultrasonics 29, 464 (1991).
[13] A. Korpel, Appl. Phys. Lett. 9, 425 (1966).
[14] A. Korpel, IEEE Trans. Sonics Ultrason. SU-15, 153 (1968).
[15] A. Korpel, J. Opt. Soc. Am. 69, 678 (1979).
[16] A. Korpel and T. C. Poon, J. Opt. Soc. Am. 70, 817 (1980).
[17] T. C. Poon and A. Korpel, J. Opt. Soc. Am. 71, 1202 (1981).
[18] M. R. Chatterjee, T. C. Poon, and D. N. Sitter, Acustica 71, 81 (1990).
[19] P. P. Banerjee and C. W. Tarn, in Proceedings of Ultrasonics International '91, Le Touquet, France (Butterworth-Heinemann, Guilford, U.K., 1991), pp. 127–130.
[20] F. D. Martin, L. Adler, and M. A. Breazeale, J. Appl. Phys. 43, 1480 (1972).
[21] J. K. Na, MS thesis, University of Tennessee, Knoxville, TN, 1986.
[22] R. R. Aggarwal, Proc. Ind. Acad. Sci. Sec. A 31, 417 (1950).
[23] N. S. N. Nath, Proc. Ind. Acad. Sci. Sec. A 4, 222 (1936).
[24] A. Korpel, P. Banerjee, and C. W. Tarn, Opt. Commun. 97, 250 (1993).
[25] P. Phariseau, Proc. Ind. Acad. Sci. Sec. A 44, 165 (1956).
[26] I. Stakgold, Green's Functions and Boundary Value Problems (Wiley-Interscience, New York, 1979), p. 98.